Draft version 1.0

CEPC NOTE

CEPC_ANA_HIG_2015_XXX

August 14, 2017

Measurement of the branching ratio BR($H \to WW^*$) at CEPC

LIAO Libo[a,b], LI Gang[b], RUAN Manqi[b], LI Kang[a], and XU Qingjun[a]

[a]Hangzhou Normal University
[b]Institute of High Energy Physics

Abstract

It's a note for measurement of branch ratio BR($H \to WW^*$) .

- **Abstract:** Based on a Monte Carlo sample with planed lumonisity of $5ab^{-1}$ at CEPC, measurement of branch ratio BR($H \to WW^*$) has been performed under full simulation. In this analysis, 14 decay modes of WW^* are studied.

E-mail address: liaolb@ihep.ac.cn

Contents

1 Introduction

The precise measurement of the Higgs boson properties has become a high priority target for the particle physics community worldwide 5 years after the particle discovery [1] [2]. In order to carry out this programme at the required precision, dedicated Higgs factories are needed. The LHC is an excellent Higgs factory, which led to the Higgs boson discovery and its first property measurements. Despite its success, the LHC is limited by enormous backgrounds and large theoretical and experimental uncertainties, which limit the precision of the Higgs boson measurements to the level of 5-10%. This precision is not adequate to differentiate between the Standard Model (SM) and various new physics models [3].

On the other hand, an electron positron collider provides a unique physics opportunity to improve the precision of the Higgs boson property measurements beyond the reach of the LHC. It can measure the absolute values of the Higgs boson couplings, the Higgs boson width, and, in addition, it has unique sensitivity to Higgs boson exotic decay modes [4]. Besides, the e^+e^- collider physics programme is complementary to that of proton colliders [citation needed]. All these have stimulated the interest of the particle physics community worldwide and various different e^+e^- facilities have been proposed.

The CEPC is a circular e^+e^- collider with a circumference of 50 - 100km [5]. It is expected to deliver one million Higgs bosons, which will be detected and reconstructed with almost 100% efficiency during 10 years operation and with 2 detectors. Such a sample will allow the measurement of Higgs boson couplings with precision of 0.1–1% level, which is one order of magnitude better than the current HL-LHC expectation [6].

At the CEPC with center-mass of energy $\sqrt{s}$ = 250 GeV and non-polarized beams, Higgs bosons are produced through Higgsstrahlung [7], which dominates, and vector boson fusion, see Figure 1.

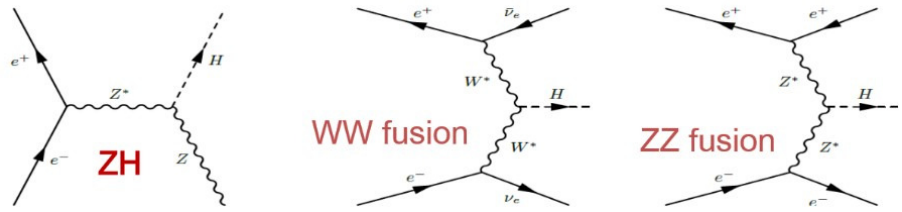

Figure 1: Feynman diagrams for Higgs boson production mechanisms at CEPC

1.1 Classification of signal final states

A full simulation study of the measurement of Br($H \to WW^*$) at the CEPC is highly motivated. Firstly, the SM Higgs boson branching ratio to WW^* is 22%, which renders is the most important channel to study the HWW coupling at the CEPC. Moreover, the Br($H \to WW^*$) measurement is also a key ingredient for the determination of the Higgs boson width. Last but not least, the W bosons decay into various physics objects (leptons, missing energy and momentum, taus and jets), providing an excellent benchmark to evaluate detector performance. The current status of the CEPC full simulation studies for the measurement of branch ratio BR($H \to WW^*$) is reported in this note.

For the studies discussed here, the $H \to WW^*$ decays are classified into 50 different channels according to the number of electrons, muons, tau-leptons, neutrinos and jets in the final state. Assuming one million Higgs bosons, the expected yield for $H \to WW^*$ events in these final states is presented in Table 1. These final states are further classified into four categories depending on the number of jets in the event. As shown in Table 1 there can be, zero, two, four or six jet events.

W boson decay \ Z boson decay	ee	$\mu\mu$	$\tau\tau$	$\nu\nu$	qq
$WW^* \to e\nu e\nu$	88	88	88	603	1836
$WW^* \to \mu\nu\mu\nu$	87	87	87	593	1808
$WW^* \to e\nu\mu\nu$	175	175	175	1206	3644
$WW^* \to e\nu\tau\nu$	187	187	188	1281	3901
$WW^* \to \mu\nu\tau\nu$	186	186	186	1271	3872
$WW^* \to \tau\nu\tau\nu$	99	99	99	681	2072
$WW^* \to e\nu qq$	1111	1112	1114	7589	23112
$WW^* \to \mu\nu qq$	1103	1104	1105	7530	22939
$WW^* \to \tau\nu qq$	1181	1182	1183	8066	24558
$WW^* \to qqqq$	3498	3502	3506	23884	72735

Table 1: Signal events of the $Z \to X, H \to WW^*, WW^* \to X$ processes. The different colours denote different jet categories: zero-jet category (gray), two-jet category (green), four-jet category (magenta), and six-jet category (red).

In this note, a representative analysis of each jet category is reported in detail. For the zero-jet category, $e^+e^- \to ZH, Z \to \mu^+\mu^-, H \to WW^*, WW^* \to e\nu\mu\nu$ decay chain has been considered. For categories with jets the following decay chains have been studied: $e^+e^- \to ZH, Z \to e^+e^-, H \to WW^*, WW^* \to \mu\nu qq$ (two-jet category) and $e^+e^- \to ZH, Z \to \nu\nu, H \to WW^*, WW^* \to qqqq$ (four-jet category). The six-jet category is more complicated and will be the topic of a future analysis.

2 MC samples

2.1 Simulation and analysis tools

This analysis is performed using simulated data that correspond to an integrated luminosity of 5000fb^{-1} at $\sqrt{s} = 250$ GeV. The cross section and No. of events for the various processes relevant for this energy is shown in Figure 2 and Table 2. For all signal samples a Higgs boson mass of $m_H = 125$ GeV is assumed. Background events are generated by Whizard 1.95 [8] and include initial state radiation (ISR). The detector model, cepc_v1 [5], is simulated by `Geant4` [9]. Object reconstruction is done using the particle-flow algorithm, `Arbor` [10]. Charged particle identification is performed by LICH [11], which is a TMVA-based [12] software package optimized for a high granularity calorimeter [13]. The *ee*-k_T clustering algorithm is used for jet clustering and the performance of the b-tagging algorithm is given by LCFIPlus package [14].

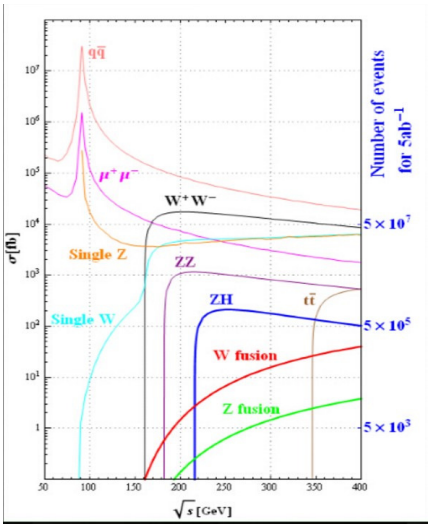

Figure 2: The distribution of cross section of the Standard Model when center mass of system is near 250 GeV.

Process	Cross Section in fb	Number of Events in 5000fb^{-1}
Higgs production		
ZH	212	1.06×10^6
$\nu\bar{\nu}H$	6.27	3.36×10^4
e^+e^-H	0.63	3.15×10^3
total	219	1.10×10^6
Standard Model Background		
qq	50216	2.5×10^8
$\mu\mu$	4405	2.2×10^7
WW	15484	7.7×10^7
ZZ	1033	5.2×10^6
eeZ(single Z)	4734	2.4×10^7
$e\nu W$(single W)	5144	2.6×10^7
total	801016	3.54×10^8

Table 2: The specific value of cross section and No. of events of the signal processes and the main Standard Model when center mass of system is 250 GeV.

The SM backgrounds included in this search are classified in two-fermion and four-fermion final states. Two fermion backgrounds include Bhabha scattering and the production of $\mu^+\mu^-$, $\tau^+\tau^-$, $\nu\bar{\nu}$ and $q\bar{q}$ pairs. Four fermion background consist of rest of the SM backgrounds. This includes also ZH production in which the Higgs boson decays to channels other than WW.

2.2 Pre-selection

The total background to the branching ratio measurement amounts to more than 30 million events according to Table 2. Many of those events, however, have completely different topologies compared to

signal, and therefore the decision to reject them can be made at an early stage, even before the simulation.

The events are categorized to four classes: $llH(l = e, \mu)$, $\tau\tau H$, $\nu\nu H$ and qqH. Subsequently, a loose selection is performed on the objects before they are passed to the full detector simulation, which will be referred to in the following as pre-selection. The pre-selection is such that it is fully efficient for signal events.

2.2.1 Pre-selection of $e^+e^- \to ZH, Z \to l^+l^-(l = e, \mu), H \to X$ decay

Compared to the SM background, the most distinguishing feature of $Z \to l^+l^-(l = e, \mu), H \to X$ decays is the invariant mass and the recoil mass of Z boson. For the pre-selection, all the leptons with same flavor would be looped, and two of them which combined invariant mass is nearest to mass of Z boson are selected. And subsequently a window in the di-lepton invariant mass and in the recoil mass is required with numerical values shown in Table 3.

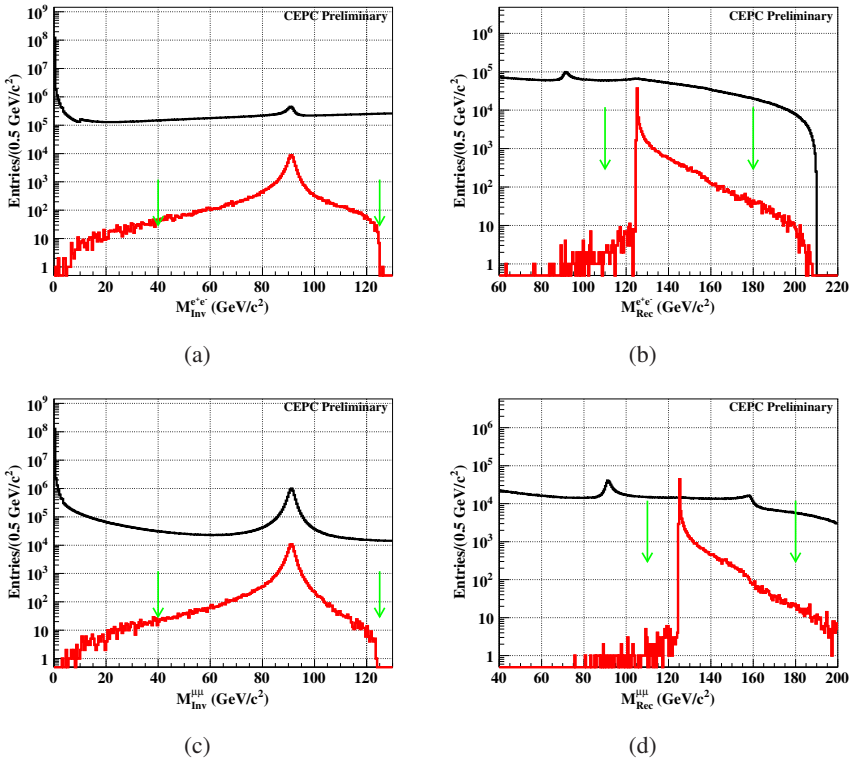

Figure 3: The distribution of invariant mass and recoil mass of the best candidate of Z boson. Red line is the distribution of Higgs signal. Black line is the distribution of the Standard Model background. TOP: These two plots are the mass distribution of $Z \to e^+e^-, H \to X$ decay. Bottom: The left is invariant mass distribution and right is recoil mass distribution of $Z \to \mu^+\mu^-, H \to X$ decay.

After applied the pre-selection in MC level and full simulated, the same variable of pre-selection should be valid, as shown in Figure 4, and the cut windows shown in Table 3.

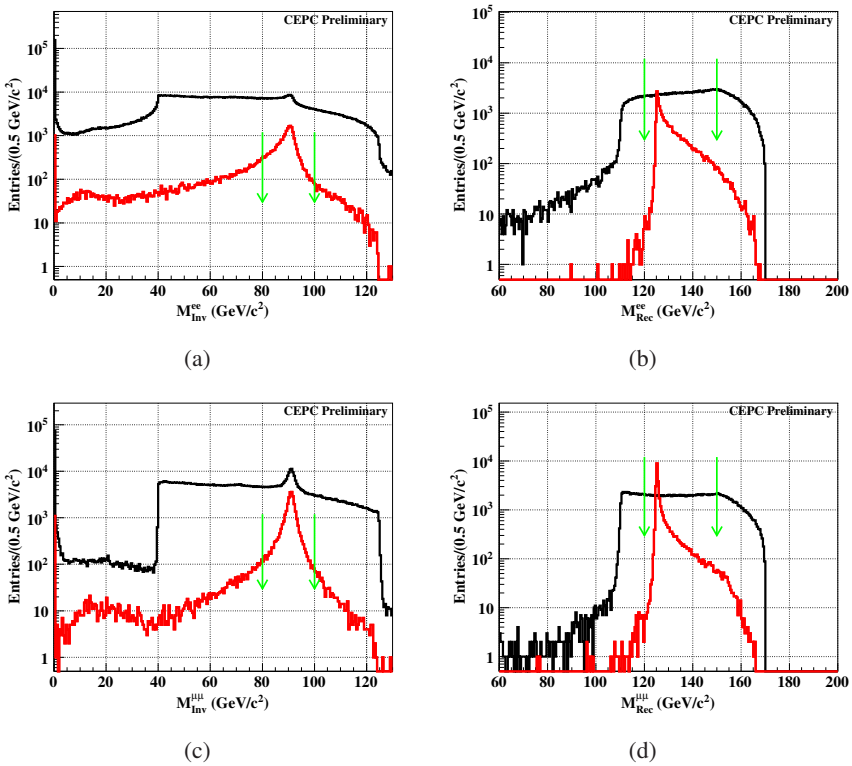

Figure 4: The distribution of invariant mass and recoil mass of the best candidate of Z boson in full simulation. Red line is the distribution of Higgs signal. Black line is the distribution of the Standard Model background. TOP: These two plots are the mass distribution of $Z \to e^+e^-, H \to X$ decay. Bottom: The left is invariant mass distribution and right is recoil mass distribution of $Z \to \mu^+\mu^-, H \to X$ decay.

Process of signal	eeH process	$\mu\mu H$ process
conditions of pre-selection	$40\ \mathrm{GeV}/c^2 < M^{ee}_{Inv} < 130\ \mathrm{GeV}/c^2$ $110\ \mathrm{GeV}/c^2 < M^{ee}_{Rec} < 180\ \mathrm{GeV}/c^2$	$40\ \mathrm{GeV}/c^2 < M^{\mu\mu}_{Inv} < 130\ \mathrm{GeV}/c^2$ $110\ \mathrm{GeV}/c^2 < M^{\mu\mu}_{Rec} < 180\ \mathrm{GeV}/c^2$
conditions of validation	$80\ \mathrm{GeV}/c^2 < M^{ee}_{Inv} < 100\ \mathrm{GeV}/c^2$ $120\ \mathrm{GeV}/c^2 < M^{ee}_{Rec} < 150\ \mathrm{GeV}/c^2$	$80\ \mathrm{GeV}/c^2 < M^{\mu\mu}_{Inv} < 100\ \mathrm{GeV}/c^2$ $120\ \mathrm{GeV}/c^2 < M^{\mu\mu}_{Rec} < 150\ \mathrm{GeV}/c^2$

Table 3: Conditions of pre-selection in MC and validation in full simulation. Considered the resolution of detector, the conditions of validation should be more strict.

This pre-selection is highly efficient for signal: more than 95% of signal event are retained. At the same time more than 99% of the background events are rejected.

2.2.2 Pre-selection of $e^+e^- \to ZH, Z \to \nu\bar{\nu}, H \to X$ decay.

The pre-selection of $\nu\nu H$ channel is less trivial to define compared to eeH and $\mu\mu H$ decay chains. Due to the $Z \to \nu\nu$ decay, it is possible to use the missing mas of the event to discriminate between signal and background. In addition to the missing mass, the total mass and the total transverse momentum are used, as well as the polar angle of each final state particle $|cos\theta| < 0.99$ is contained.

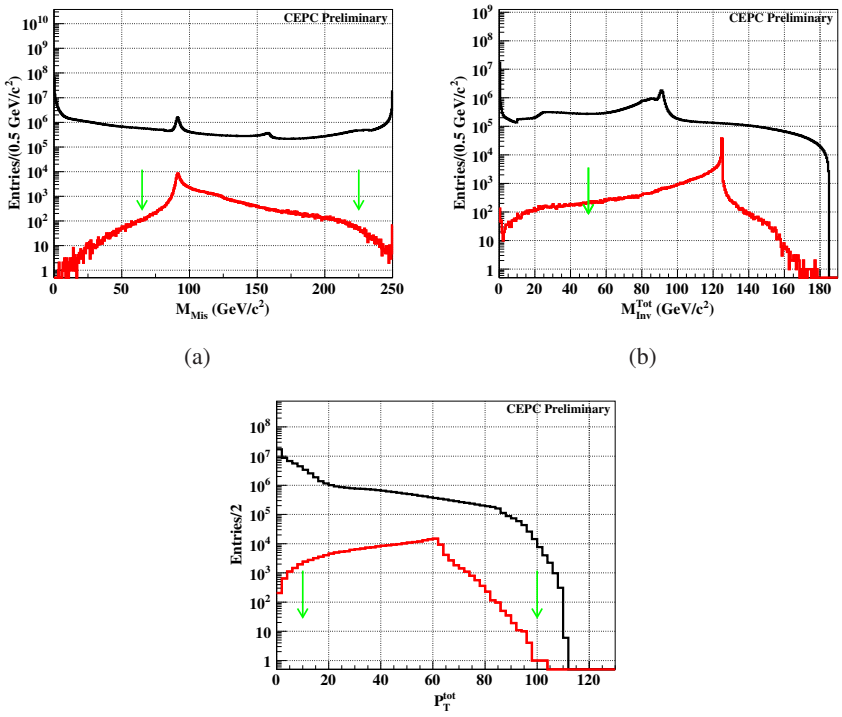

Figure 5: The distribution of missing mass, total mass and total transverse momentum in MC truth. Red line is the distribution of Higgs signal. Black line is the distribution of the Standard Model background. Top: The left is missing mass of event. The right is total mass of event. Bottom: It is the distribution of total transverse momentum of event.

As same as the $Z \to ll$ decay channel, after applied the pre-selection in MC, the same variable should be valid in full simualtion.

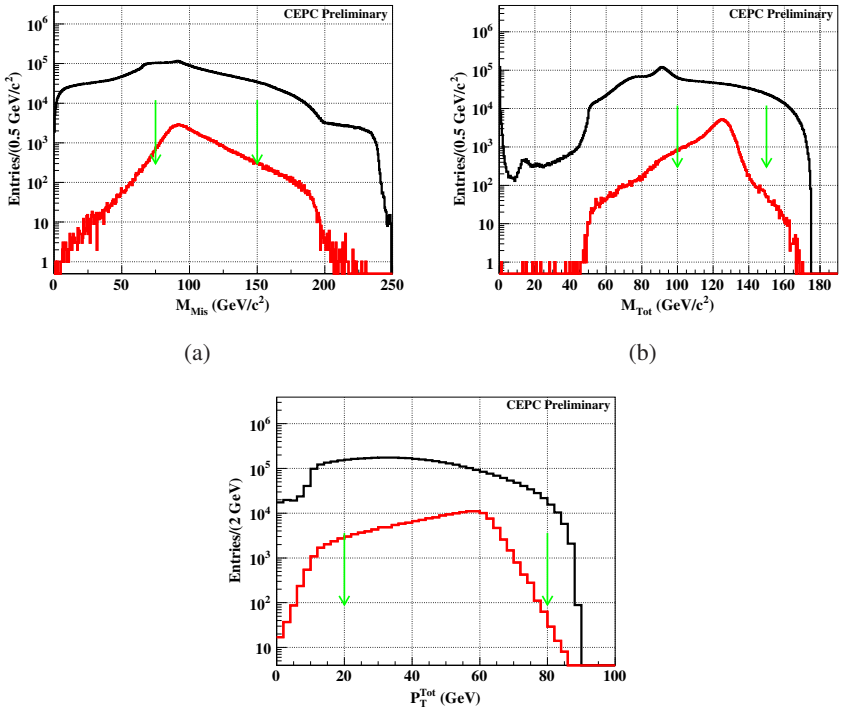

Figure 6: The distribution of missing mass, total mass and total transverse momentum in full simulation. Red line is the distribution of Higgs signal. Black line is the distribution of the Standard Model background. Top: The left is missing mass of event. The right is total mass of event. Bottom: It is the distribution of total transverse momentum of event.

Process of signal	$\nu\nu H$
conditions of pre-selection	$65\ \mathrm{GeV}/c^2 < M_{Mis} < 225\ \mathrm{GeV}/c^2$ $M_{Tot} > 50\ \mathrm{GeV}/c^2$ $10\ \mathrm{GeV}/c < p_T < 100\ \mathrm{GeV}/c$
conditions of validation	$75\ \mathrm{GeV}/c^2 < M_{Mis} < 150\ \mathrm{GeV}/c^2$ $100\ \mathrm{GeV}/c^2 < M_{Tot} < 150\ \mathrm{GeV}/c^2$ $20\ \mathrm{GeV}/c < p_T < 80\ \mathrm{GeV}/c$

Table 4: Conditions of pre-selection in MC and validation in full simulation of $\nu\nu H$ process

The distributions of signal and background events are similar, as shown in Figure 5. The pre-selection conditions are defined in Table 2.2.2 and take into account this feature.

The distribution of the same variables after reconstruction is shown in Figure 6. Considering the resolution of detector, the conditions of pre-selection should be valided more strict in full simulation.

3 Measurement of $Br(H \to WW^*)$

After the pre-selection is defined, the sensitivity estimation of the measurement of the branching ratio can proceed. Due to the large number of possible decay chains only a subset of them will be considered in the following, as discussed earlier.

3.1 Analysis of $e^+e^- \to ZH, Z \to \mu^+\mu^-, H \to WW^*, WW^* \to e\nu\mu\nu$ decay

3.1.1 Event selection

The $e^+e^- \to ZH, Z \to \mu^+\mu^-, H \to WW^*, WW^* \to e\nu\mu\nu$ channel is selected because it contains two different flavour leptons in the final state, which can be used very effectively to supress the backgrounds.

The requirement of exactly three muons and one electron and less than three remain neutral particles in the event has been shown in Ref. [15] to allow only small backgrounds due to $ZZ \to \mu^+\mu^-\tau^+\tau^-$ and $ZZ \to 4\tau$ decays. Hence, the main background is due to other Higgs boson decays, such as $H \to \tau\tau$.

To cut down these Higgs background and ZZ events background, the combined invariant mass of e and μ within 10 GeV/c^2 and 65 GeV/c^2, and missing mass of event less than 65 GeV/c^2, are applied.

The SM background is further reduced by the expected excellent performance of the CEPC vertex detector (VTX), which is planned to be constructed with high resolution pixel sensors near the interaction point(IP) resulting in resolution better than $4\mu m$. By requiring $\sqrt{(\frac{D_0}{sigD_0})^2 + (\frac{Z_0}{sigZ_0})^2} < 5$ for e and μ decayed from W boson, D_0 and $sigD_0$ showed the derivation in X-Y plane, Z_0 and $sigZ_0$ showed the derivation in Z direction, it is efficient to discriminate the background events of τ leptons or heavy flavour quarks.

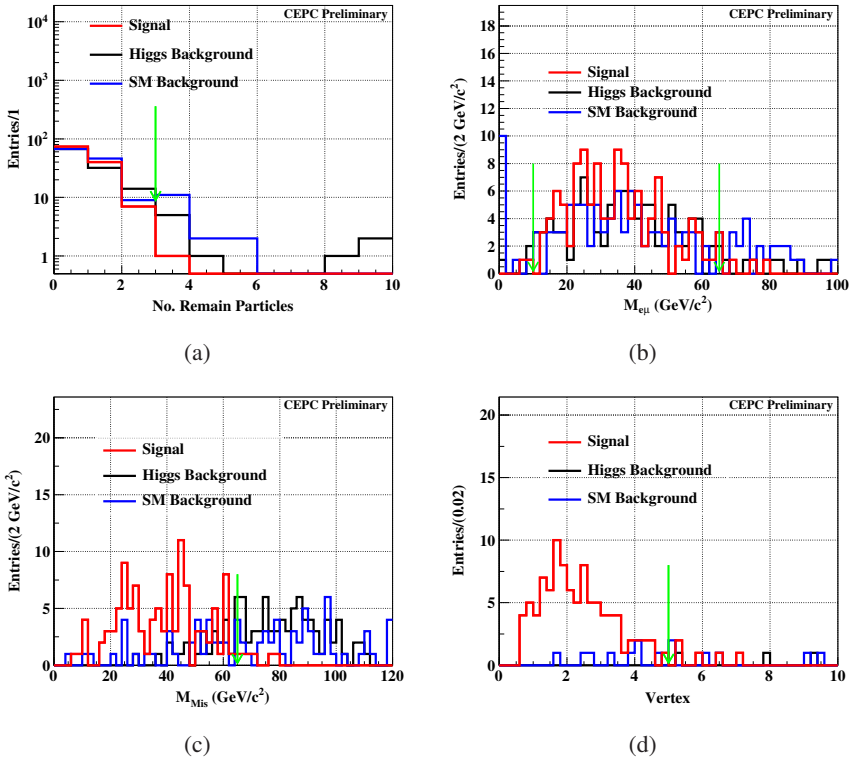

Figure 7: 7(a) The No. remain particles of $e^+e^- \to ZH, Z \to \mu^+\mu^-, H \to WW^*, WW^* \to e\nu\mu\nu$ decay. Except for four tracks, there are few photons, so we can veto semi-leptonic decay and hadronic decay of background. 7(b) The distribution of combined invariant mass of electron and muon. Since these two leptons decayed from different W boson, the combined invariant mass of them should be less than the mass of on-shell W boson. 7(c) The distribution of missing mass of event. Since there are two neutrinos in this signal process and much more neutrinos in background, four in ZZ background and $H \to \tau\tau$ background, the missing mass should be less than them. 7(d) The distribution of Vertex of $e^+e^- \to ZH, Z \to \mu^+\mu^-, H \to WW^*, WW^* \to e\nu\mu\nu$ decay. And there are two leptons totally from W boson, so we plus the value of each lepton. And leptons from τ and b-jet would fly a long distance, so they would be rejected effectively.

147 The number of events passing each selection step is shown in Table 5. The main background of this
148 channel comes from the $e^+e^- \to ZZ \to \tau^+\tau^-\mu^+\mu^-$ process, as shown in Table 6.

Category	Signal	ZH background	SM background
Total	172	34624	700311
Validation of pre-selection	136	29263	117395
$N_{ZPole} = 2; N_{Isolep} = 2; l_1 = e, l_2 = \mu$	122	145	150
$N_{Remain} < 3$	121	113	122
10 GeV $< M_{Inv}^{e\mu} <$ 65 GeV	116	101	87
$M_{Missing} < 65$ GeV$/c^2$	110	26	36
$\sqrt{(\frac{D0}{sigD0})^2 + (\frac{Z0}{sigZ0})^2} < 5$	93	3	10

Table 5: The final event selection of $e^+e^- \to ZH, Z \to \mu^+\mu^-, H \to WW^*, WW^* \to e\nu\mu\nu$ decay.

Decay Chain	Final States	Number of Events
$e^+e^- \to ZZ, ZZ \to \tau^+\tau^-\mu^+\mu^-$	$\mu^+, \mu^-, \tau^+, \tau^-$	10

Table 6: Summery of total background with the same final states of signal event

3.1.2 Statistical result

The distribution of the recoil mass of the $\mu^+\mu^-$ system after the selection is shown in Figure 8.

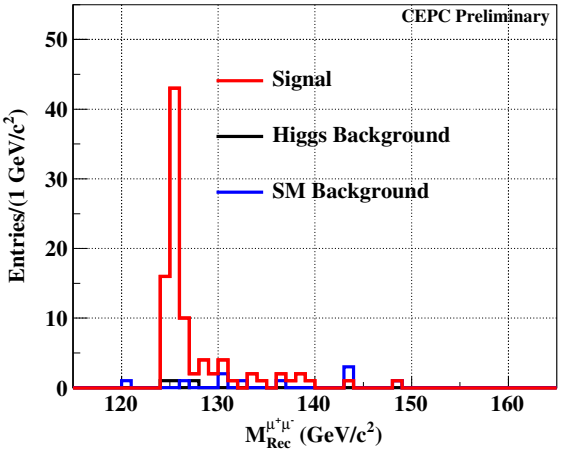

Figure 8: The distribution of recoil mass of $\mu^+\mu^-$ after event selection

The final number of signal events is estimated to be $N_{sig} = 93 \pm 10$ with a selection efficiency of $\varepsilon = 54.1\%$. Hence, the expected sensitivity of the measurement for this channel is:

$$Accu. = \frac{\sqrt{S+B}}{S} = 10.7\%.$$

3.2 Analysis of $e^+e^- \to ZH, Z \to e^+e^-, H \to WW^*, WW^* \to \mu\nu q\bar{q}$ decay

3.2.1 Event selection

This channel is more promising for a high precision measurement compared to the $ZWW^* \to \mu\mu\mu\nu e\nu$ channel discussed in the previous section due to the larger branching ratios involved. The final state consists of three leptons, several jets and neutrinos. The fully leptonic decay background and full hadronic decay can be reduced a lot by requiring the number of remain particles, $7 < N_{Remain} < 30$, except for three energetic leptons.

In this final state, the most effective criteria to supress the SM background in pre-selection are the invariant mass and the recoil mass of the ee system. The constraints $80\ \mathrm{GeV}/c^2 < M_{Inv}^{e^+e^-} < 100\ \mathrm{GeV}/c^2$ and $120\ \mathrm{GeV}/c^2 < M_{Rec}^{e^+e^-} < 150\ \mathrm{GeV}/c^2$ are, hence, required, as part of the channel pre-selection.

Differences in the di-jet system between Higgs, W and Z boson deacys as well as hadroni τ lepton decays can be exploited to reduce backgrounds. In particular, the invariant mass of the di-jet system is required to be $10\ \mathrm{GeV}/c^2 < M_{Rec}^{di-Jet} < 95\ \mathrm{GeV}/c^2$. In addition, b-tagging is used to veto backgrounds with b-jets.

The excellent expected CEPC tracking performance is exploited to distinguish muons from W and muons from τ lepton decays using the requirement $\sqrt{(\frac{D_0}{sigD_0})^2 + (\frac{Z_0}{sigZ_0})^2} < 4$. In addition, in order to veto

background from the t-channel because there are lots of t-channel background according to Feynman diagram, a transverse momentum requirement $p_T > 5$ GeV is applied.

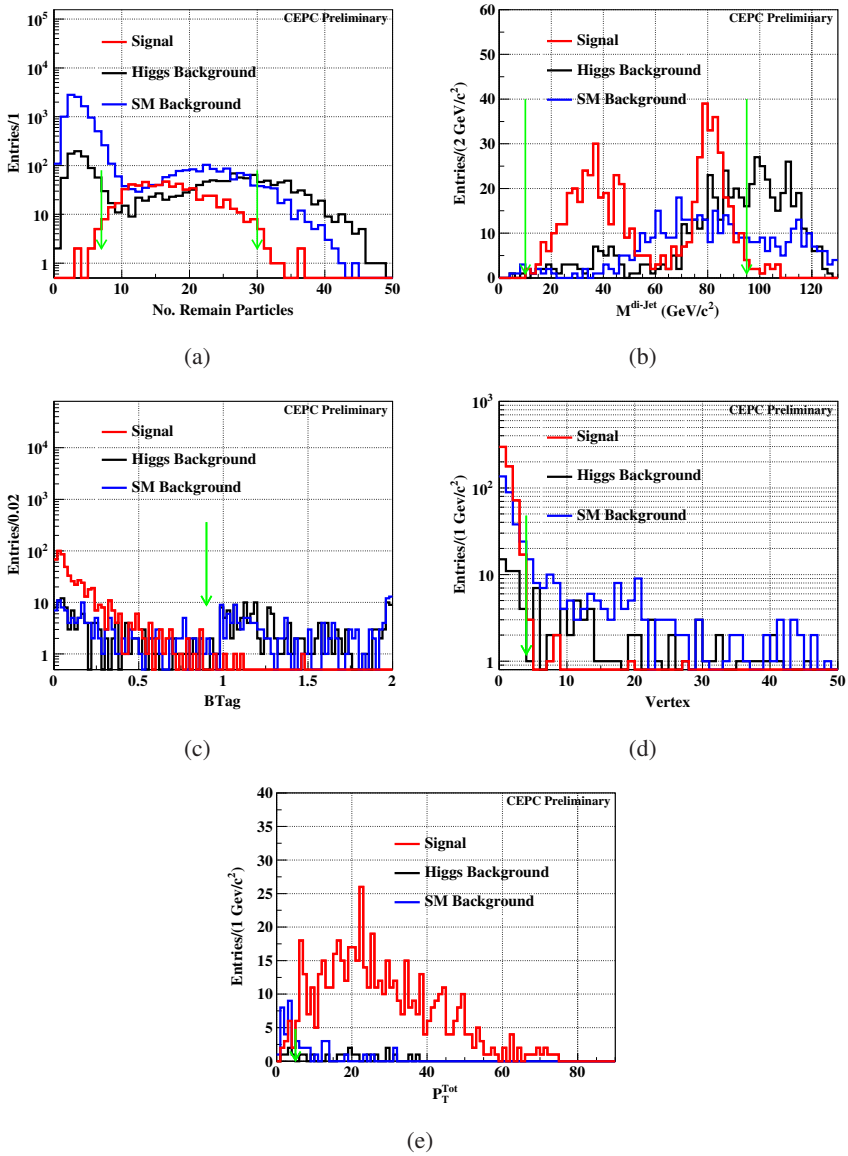

Figure 9: 9(a) The No. remain particles of $e^+e^- \to ZH, Z \to e^+e^-, H \to WW^*, WW^* \to \mu\nu q\bar{q}$ decay. Because it is semi-leptonic decay channel, so the No. remain particles should between it of hadronic decay and full-leptonic decay. 9(c) The distribution of Btag, we plus the Btag value of each jets because of existing two jets. And because no b-jet decay from W boson, the value of them should be less than 1. 9(d) The distribution of vertex of lepton. Leptons from τ and b-jet would fly a long distance, so they would be rejected effectively. 9(e) The distribution of transverse momentum p_T. Transverse momentum of t channel would be lower than of s channel. 9(b) The distribution of di-jet invariant mass, the high-side could distinguish the jets from Z boson or H boson.

The selection criteria, as well as the signal and background events passing each of them, are summarized in in Table 7. The main backgrounds after the full selection are shown in Table 8, and only background which remain number is larger than ten would be regarded as main background.

Category	Signal	ZH background	SM background
Total	1149	36319	1303847
$N_{ZPole} = 2; N_{Isolep} = 1; N_{Jets} = 2; l = \mu$	1022	1970	21857
Validation of pre-selection	631	1207	2987
$7 < N_{Remain} < 30$	603	540	436
$15\ \mathrm{GeV}/c^2 < M_{Rec}^{di-Jet} < 95\ \mathrm{GeV}/c^2$	589	284	278
$Btag < 0.9$	584	116	131
$M_{Missing} < 45\ \mathrm{GeV}/c^2$	571	72	102
$\sqrt{(\frac{D0}{sigD0})^2 + (\frac{Z0}{sigZ0})^2} < 4$	564	23	45
$p_T > 5$ GeV	551	18	21

Table 7: The final event selection of $e^+e^- \to ZH, Z \to e^+e^-, H \to WW^*, WW^* \to \mu\nu q\bar{q}$ decay

Decay Chain	Final States	Number of Events
$e^+e^- \to ZH, Z \to e^+e^-, H \to WW^* \to \tau\nu q\bar{q}$	$e^+, e^-, \tau, \nu, 2q$	14
$e^+e^- \to e^+e^-Z, Z \to qq$	$e^+, e^-, 2q$	13

Table 8: Summery of total background with the same final states of signal event

3.2.2 Statistical result

After selection, the distribution of the recoil mass of the e^+e^- system is shown in Figure 10.

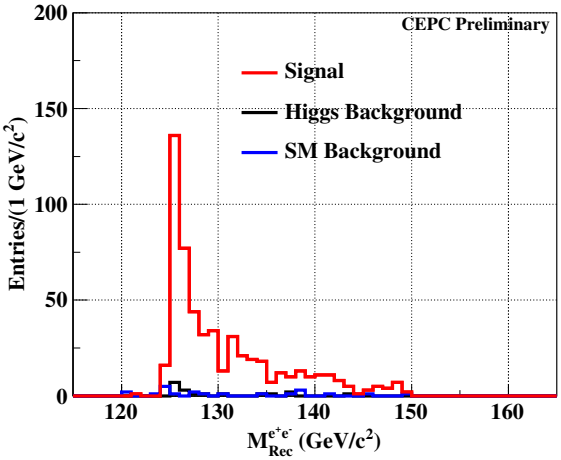

Figure 10: The distribution of recoil mass of e^+e^- after event selection

The final number of signal events is found to be $N_{sig} = 551 \pm 24$ and the selection efficiency is $\varepsilon = 48.0\%$. Hence, the expected sensitivity of the measurement for this channel is:

$$Accu. = \frac{\sqrt{S+B}}{S} = 4.5\%.$$

3.3 Analysis of $e^+e^- \to ZH, Z \to \nu\bar{\nu}, H \to WW^*, WW^* \to q\bar{q}q\bar{q}$ decay

3.3.1 Event selection

This is a hadronic channel that features no leptons, light flavour jets and large missing transverse energy. The SM background is reduced by vetoing events with isolated leptons and by requiring at least two jets. The event particle multiplicity is required to be large, $N^{\text{Total}}_{\text{Particles}} > 20$, due to the many hadrons produced after the quark hadronization takes place.

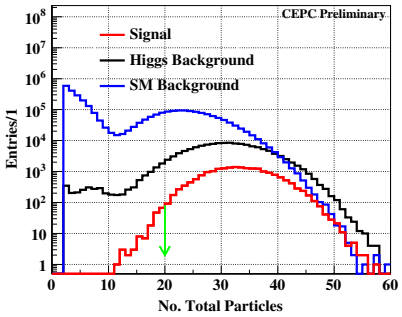

Figure 11: The number of total final particles distribution. To count the total number, the energy threshold of each particle is required, $E > 1$ GeV

[It is not clear how this process is done, please clarify.(just do jet clustering twice.)] For this study, jet selection is done in two steps. In the first step, two jets are required in the event to discriminate against two-jet background, such as $H \to q\bar{q}$ decays, ZZ semi-leptonic decays and single-$Z\nu$ semi-leptonic decays. The jets jets are required to satisfy $Btagging < 0.9$, $Cos\theta_{2jets} > 0.87$ and $\Sigma|M^{2jet}_{Inv}| > 50$ GeV/c^2. *Btagging* means the probilities of flavor tagging for each jet and sum them up. $Cos\theta_{2jets}$ means the cos angle of this two jets. $\Sigma|M^{2jet}_{Inv}|$ means sum the invariant mass of each jet. In the second step, four jets are required in the event. This category is more important, since it is the feature of the signal. The event is required to satisfy $Y_{34} > 0.005$, which ycut [16] means the distances between all jets i and j. Subsequently, the four jets are used to form all possible jet pairs and the jet-jet system invariant mass is examined. The jet-jet pair with invariant mass closest to the W boson mass is taken as the on-shell W boson decay of the signal decay chain. The remaining two jets are assigned to the off-shell W boson decay. The invariant mass distribution of the two jet-jet pairs is shown in Figure 13(b). In addition, the following conditions are required to be met by the jet-jet pairs:

- $65\ \text{GeV}/c^2 < M^{Real4jet}_{Inv} < 85\ \text{GeV}/c^2$,
- $15\ \text{GeV}/c^2 < M^{Virt4jet}_{Inv} < 50\ \text{GeV}/c^2$,
- $M^{Virt4jet}_{Inv} > -7/3M^{Real4jet}_{Inv} + \frac{605}{3}\ \text{GeV}/c^2$,

where $M^{Real4jet}_{Inv}$ ($M^{Virt4jet}_{Inv}$) is the invariant mass of the jet-jet system assigned to the on-shell (off-shell) W boson decay.

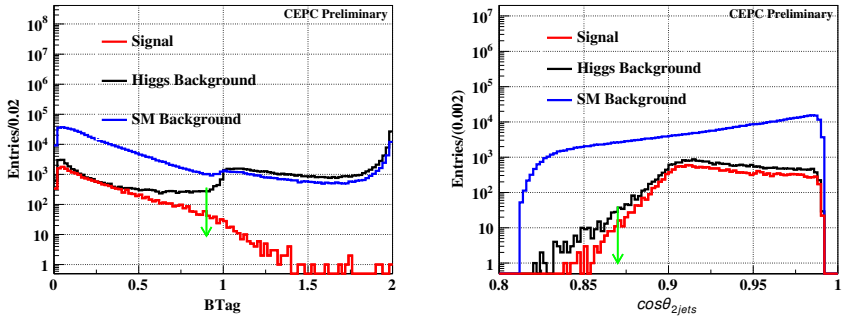

(a)

(b)

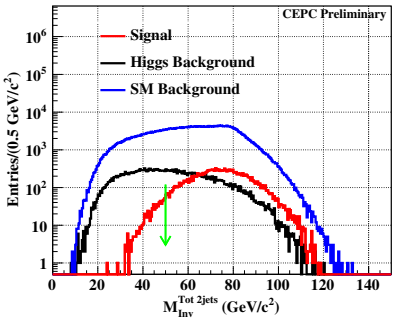

(c)

Figure 12: 12(a) B-tag of two jets distribution. We plus the value of B-tag of each jet, 12(b) The distribution of angle between two jets. The boost of Higgs is larger, so the angle between two jets in signal should be smaller its in background. 12(c) The distribution of total invariant mass of two jets. The number of jets in almost background is two. The invariant mass of each jet should be smaller.

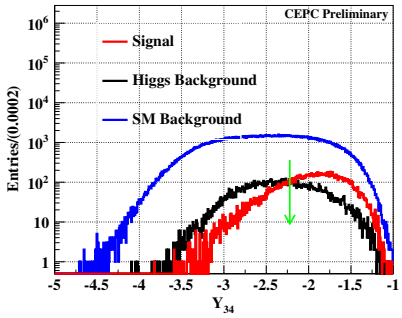

(a)

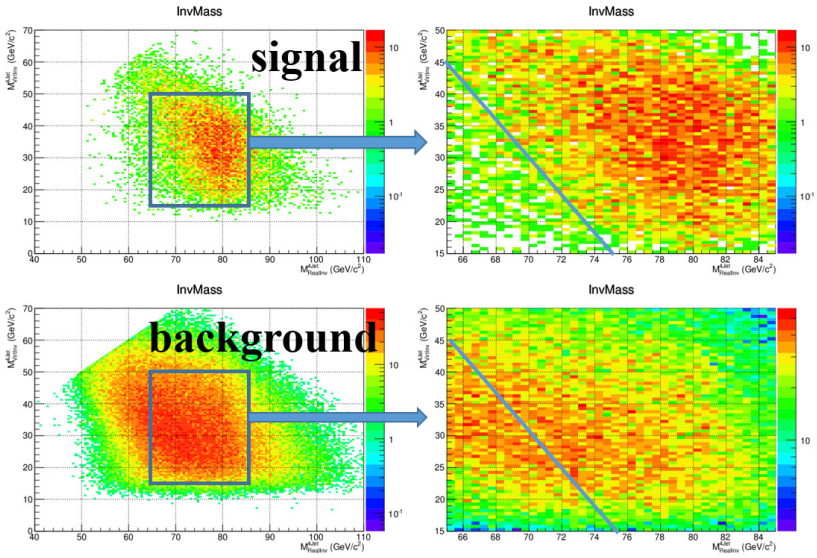

(b)

Figure 13: 13(a) Y value distribution. 13(b) 2D scatter diagram of invariant mass of real and virtual W boson. The left plot represents the distribution of signal, and the right is of background. In order to distinguish the signal and background effectively, a hexagonal mass window is applied.

198 The event selection steps as well as the number of signal and background events passing each step is
199 shown in Table 9. The signal efficiency for this selection is about 50%.

Category	Signal	ZH background	SM background
Total	23938	208200	21314314
Validation of pre-selection	20405	143765	3166923
$N^{Tot}_{Particle} > 20$	19681	124112	537839
$Btag < 0.9$	19349	28857	477099
$Cos\theta_{2jets} > 0.87$	19298	28673	433563
$\Sigma\lvert M^{2jet}_{Inv}\rvert > 50$ GeV	18621	14793	309919
$Y_{34} > 0.005$	15183	6919	122866
Combined Variable	9022	3075	38226

Table 9: The final event selection of $e^+e^- \to ZH, Z \to \nu\bar{\nu}, H \to WW^*, WW^* \to q\bar{q}q\bar{q}$ decay

Decay Chain	Final States	Number of Events
$e^+e^- \to ZH, Z \to \nu\bar{\nu}, H \to c\bar{c}$	$\nu, \bar{\nu}, c, \bar{c}$	192
$e^+e^- \to ZH, Z \to \nu\bar{\nu}, H \to b\bar{b}$	$\nu, \bar{\nu}, b, \bar{b}$	352
$e^+e^- \to ZH, Z \to \nu\bar{\nu}, H \to gg$	$\nu, \bar{\nu}, 2g$	2028
$e^+e^- \to ZH, Z \to \nu\bar{\nu}, H \to ZZ^*, ZZ^* \to q\bar{q}q\bar{q}$	$\nu, \bar{\nu}, 2q, 2\bar{q}$	439
$e^+e^- \to ZZ, ZZ \to \nu\bar{\nu}q\bar{q}$	$\nu, \bar{\nu}, 2q$	3115
$e^+e^- \to ZZ, ZZ \to \tau^+\tau^- q\bar{q}$	$\tau^+, \tau^-, 2q$	910
$e^+e^- \to WW, WW \to \tau\nu qq$	$\tau, \nu, 2q$	30398
$e^+e^- \to WW, WW \to \mu\nu qq$	$\mu, \nu, 2q$	277
$e^+e^- \to \nu\bar{\nu}Z, Z \to qq$	$\nu, \bar{\nu}, 2q$	1838
$e^+e^- \to e\nu W, W \to e\nu qq$	$e, \nu, 2q$	1398
$e^+e^- \to qq$	$2q$	262

Table 10: Summery of main background with the same final states of signal event

3.3.2 Statistical result

The missing mass distribution after the selection is shown in Figure 14.

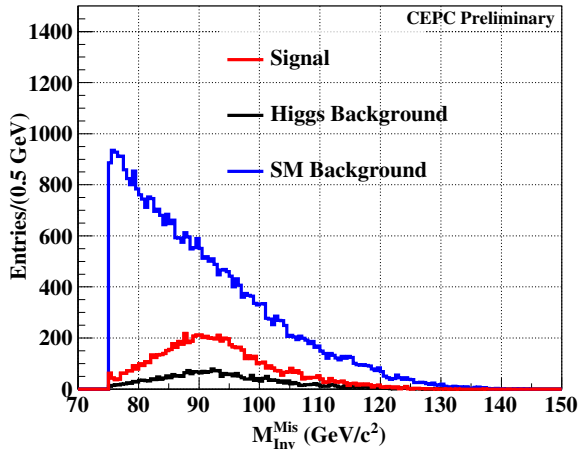

Figure 14: The distribution of recoil mass of missing mass of event after event selection

The final number of signal events is found to be $N_{sig} = 9022 \pm 224$ and the signal efficiency is $\varepsilon = 37.7\%$. Hence, the expected sensitivity of the measurement for this channel is:

$$Accu. = \frac{\sqrt{S+B}}{S} = 2.5\%.$$

4 Results

The final result of precision for the branching ratio BR($H \to WW^*$) is obtained using the relation:

$$\Delta Br(H \to WW^*)/Br(H \to WW^*) = \sqrt{(\frac{\Delta N_{obs.}}{N_{obs.}})^2 + (\frac{\Delta N_{total}}{N_{total}})^2 + (\frac{\Delta Br_{rel.}}{Br_{rel.}})^2},$$

where N_{total} and ΔN_{total} are the total number of $ee \to ZH$ producted events and its deviation, $N_{obs.}$ and $\Delta N_{obs.}$ are the number of signal events after selection and its deviation in this sample, and finally, $Br_{rel.}$ and $\Delta Br_{rel.}$ included branch fraction of Z boson and W boson and its deviation which are given by PDG table [17] and listed in Table 12. And these precisions are neligible, therefore a equation would be got:

$$\Delta Br(H \to WW^*)/Br(H \to WW^*) \sim \sqrt{(\frac{\Delta N_{obs.}}{N_{obs.}})^2}. \quad (1)$$

Then, define the vairable Γ_i as the precision of each subchannel, Γ_{ij} as the combination of two subchannels. The result of combination is:

$$\Gamma_{ij}^2 = \frac{\Gamma_i^2 \Gamma_j^2}{\Gamma_i^2 + \Gamma_j^2}. \quad (2)$$

The relative uncertainty for the number of signal events is shown in Table 11.

Category	Signal	Relative uncertainty	Efficiency of selection
$Z \to e^+e^-; H \to WW^* \to evev$	20±7	35.0%	25.0%
$Z \to e^+e^-; H \to WW^* \to \mu\nu\mu\nu$	44±8	18.2%	43.1%
$Z \to e^+e^-; H \to WW^* \to ev\mu\nu$	53±8	15.1%	27.6%
$Z \to e^+e^-; H \to WW^* \to evqq$	435±23	5.3%	37.0%
$Z \to e^+e^-; H \to WW^* \to \mu\nu qq$	551±24	4.5%	48.0%
$Z \to \mu^+\mu^-; H \to WW^* \to evev$	23±5	21.7%	25.8%
$Z \to \mu^+\mu^-; H \to WW^* \to \mu\nu\mu\nu$	39±7	17.9%	44.8%
$Z \to \mu^+\mu^-; H \to WW^* \to ev\mu\nu$	93±10	10.7%	54.1%
$Z \to \mu^+\mu^-; H \to WW^* \to evqq$	573±25	4.0%	51.7%
$Z \to \mu^+\mu^-; H \to WW^* \to \mu\nu qq$	756±30	4.4%	68.4%
$Z \to \mu^+\mu^-; H \to WW^* \to qqqq$	±	2.9%	
$Z \to \nu\bar{\nu}; H \to WW^* \to evqq$	680±32	4.7%	9.8%
$Z \to \nu\bar{\nu}; H \to WW^* \to \mu\nu qq$	790±43	4.2%	11.2%
$Z \to \nu\bar{\nu}; H \to WW^* \to qqqq$	9022±224	2.5%	37.7%

Table 11: Statistic uncertainty of Signal and Relative uncertainty

	Total events N	$Br(W \to \ell\nu)$	$Br(W \to qq)$	$Br(Z \to \ell^+\ell^-)$	$Br(Z \to qq)$
Mean value	1060000	10.86%	67.41%	3.3658%	69.91%
Uncertainty	±4000	±0.09%	±0.27%	±0.0023%	±0.06%

Table 12: Relative data for measurement of branch ratio

Through applied the Equ 1 and Equ 2, he overall combination results in a statistical uncertainty for $\Delta Br(H \to WW^*)/Br(H \to WW^*)$ is 1.29%.

5 Summary and conclusion

In summary, eleven different final states originating from $H \to WW^*$ decays have been analyzed at CEPC. The study assumes an integrated luminosity of 5000fb^{-1} and a SM Higgs boson with mass of

125 GeV. The obtained result indicates that the branching ratio BR($H \to WW^*$) can be measured with an uncertainty of just 1.29%.

	Yield events of signal process	Analyzed data
$Z \to ll, WW^* \to lvlv$	2467	28.37%
$Z \to ll, WW^* \to lvqq$	10224	43.33%
$Z \to ll, WW^* \to qqqq$	10506	33.33%(Yuqian)
$Z \to \nu\nu, WW^* \to lvlv$	4910	0%
$Z \to \nu\nu, WW^* \to lvqq$	20199	65.22%
$Z \to \nu\nu, WW^* \to qqqq$	20808	100%
$Z \to qq, WW^* \to lvlv$	17133	0%
$Z \to qq, WW^* \to lvqq$	70609	0%
$Z \to qq, WW^* \to qqqq$	72735	0%(Mila)
Total	229591	18.56%

Table 13: Yield events of signal process means the No. of events in MC level. Analyzed data means how many events of signal have been analyzed.

According to Table 13, this result is based on the analysis of only 18.56% of the data of $H \to WW^*$ events. And some channels with high cross section, such as $Z \to qq, WW^* \to \ell\nu\ell\nu$ and $Z \to qq, WW^* \to \ell\nu qq$, haven't been measured. With the CEPC research and development project ongoing, the result of this analysis are expected to improve further. In the future, $Z \to qq, H \to WW^* \to qqqq$ channel will be studied, which will improve the measurement of the branching ratio. In addition, the CEPC will also serve as a Z boson factory, increasing the overall physics output of the project. The large sample of Z boson decay events will provide both an opportunity for precision measurements and a detector performance benchmark to reduce systematic uncertainties.

The sensitivity estimation presented here has considered only statistical uncertainties and simple event counting for the final result. The effect of systematic uncertainties is not discussed. In addition, significant improvement in the sensitivity is expected if the shape of the signal-background discriminating variables is taken into account. Finally, improvement is also expected by a dedicated optimization of the isolated lepton finder algorithm. All these items will need to be addressed in a future study.

6 Acknowledgements

Thanks Dr. LI Gang and Dr. RUAN Manqi greatly for their guidance and their constructive arguments. And thanks my colleagues, Mr. CHEN Zhenxing and Mr. WEI Yuqian who build a good basement for me, Dr. MA Bingsong and Dr. MO Xin who are engaged in generator, simulation and reconstruction of samples, Dr. WANG Feng who help me solve some technical problems.

References

[1] ATLAS Collaboration, G. Aad et al., Phys. Lett. **B716** (2012) 1–29, arXiv:1207.7214 [hep-ex].

[2] CMS Collaboration, S. Chatrchyan et al., Phys. Lett. **B716** (2012) 30–61, arXiv:1207.7235 [hep-ex].

[3] S. P. Martin, arXiv:hep-ph/9709356 [hep-ph]. [Adv. Ser. Direct. High Energy Phys.18,1(1998)].

[4] D. Curtin et al., Phys. Rev. **D90** no. 7, (2014) 075004, arXiv:1312.4992 [hep-ph].

[5] CEPC-SPPC Study Group,.

[6] ATLAS, CMS Collaboration, A. Cakir, arXiv:1412.8503 [hep-ph].

[7] Z. Chen, Y. Yang, M. Ruan, D. Wang, G. Li, S. Jin, and Y. Ban, Chin. Phys. **C41** no. 2, (2017) 023003, arXiv:1601.05352 [hep-ex].

[8] W. Kilian, T. Ohl, and J. Reuter, Eur. Phys. J. **C71** (2011) 1742, arXiv:0708.4233 [hep-ph].

[9] GEANT4 Collaboration, S. Agostinelli et al., Nucl. Instrum. Meth. **A506** (2003) 250–303.

[10] M. Ruan and H. Videau, arXiv:1403.4784 [physics.ins-det].

[11] D. Yu, M. Ruan, V. Boudry, and H. Videau, arXiv:1701.07542 [physics.ins-det].

[12] TMVA Core Developer Team Collaboration, J. Therhaag, AIP Conf. Proc. **1504** (2009) 1013–1016.

[13] J.-C. Brient and H. Videau, eConf **C010630** (2001) E3047, arXiv:hep-ex/0202004 [hep-ex].

[14] T. Suehara and T. Tanabe, Nucl. Instrum. Meth. **A808** (2016) 109–116, arXiv:1506.08371 [physics.ins-det].

[15] X. Mo, G. Li, M.-Q. Ruan, and X.-C. Lou, Chin. Phys. **C40** no. 3, (2016) 033001, arXiv:1505.01008 [hep-ex].

[16] S. Catani, Y. L. Dokshitzer, M. Olsson, G. Turnock, and B. R. Webber, Phys. Lett. **B269** (1991) 432–438.

[17] Particle Data Group Collaboration, K. A. Olive et al., Chin. Phys. **C38** (2014) 090001.

Appendices

A Analysis of the other pure-leptonic decay

Except for a typical pure-leptonic decay channel(Chapter 3.1) mentioned before, there are five similar channels would be introduced below, $eeH \to eeev\nu$, $eeH \to eev\mu\nu$, $eeH \to ee\mu\nu\mu\nu$, $\mu\mu H \to \mu\mu ev\nu$ and $\mu\mu H \to \mu\nu\mu\nu$. Since they are highly similar, the analogous variables would be applied, number of remain particles, invariant mass of leptons from two W bosons, missing mass and the distance of particles from IP. In this section, only the distribution of addtional variable would be showed, since the distributions of same variable are similar.

A.1 Analysis of $e^+e^- \to ZH, Z \to e^+e^-, H \to WW^* \to ev\nu$ decay

Since the main background is eeZ in the SM background, to reduce it, transverse momentum p_T could be applied. As shown in Figure 15, transverse momentum of four leptons in eeZ process is lower than signal.

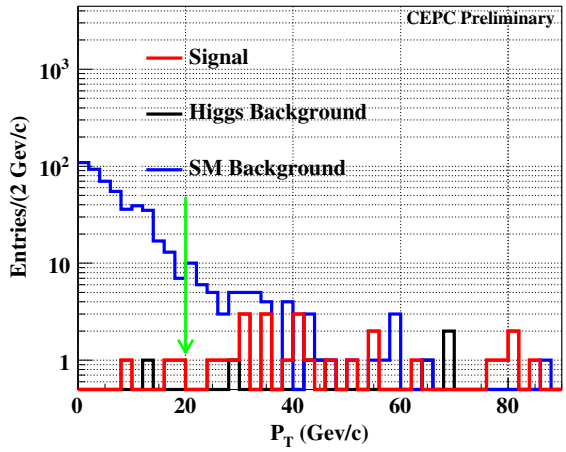

Figure 15: The distribution of transverse momentum

Cut chain of event selection in $e^+e^- \to eeev\nu$ decay channel is shown in Table 14.

Category	Signal	ZH background	SM background
Total	80	37094	1303843
Validation of Pre-selection	55	21983	151498
$N_{ZPole} = 2; N_{Isolep} = 2; l_1 = e, l_2 = e$	34	74	9725
$N_{Remain} < 5$	34	40	9417
$5\ \mathrm{GeV}/c^2 < M^{ee}_{Inv} < 45\ \mathrm{GeV}/c^2$	30	22	1724
$20\ \mathrm{GeV}/c^2 < M_{Missing} < 65\ \mathrm{GeV}/c^2$	27	7	534
$P_T > 20\ \mathrm{GeV}/c$	24	6	60
$\sqrt{(\frac{D0}{sigD0})^2 + (\frac{Z0}{sigZ0})^2} < 6$	20	1	33

Table 14: Cut chain of event selection in $e^+e^- \to eeev\nu$ decay channel

The main background and its number after event selection is shown in Table 15.

Decay Chain	Final States	Number of Events
$e^+e^- \to eeZ \to eeee$	$4e$	28

Table 15: The main background and its number after event selection

Through counting, the number of signal is $N_{sig} = 20 \pm 7$, and efficiency of signal selection is 25.0%. According to this result, the precision of this subchannel is:

$$Accu. = \frac{\sqrt{S+B}}{S} = 35.0\%.$$

A.2 Analysis of $e^+e^- \to ZH, Z \to e^+e^-, H \to WW^* \to e\nu\mu\nu$ decay

In this channel, the main background is also eeZ process, and Z boson decay to $\tau\tau$. To reduce them, transverse momentum of four leptons is also applied, shown in Figure 16

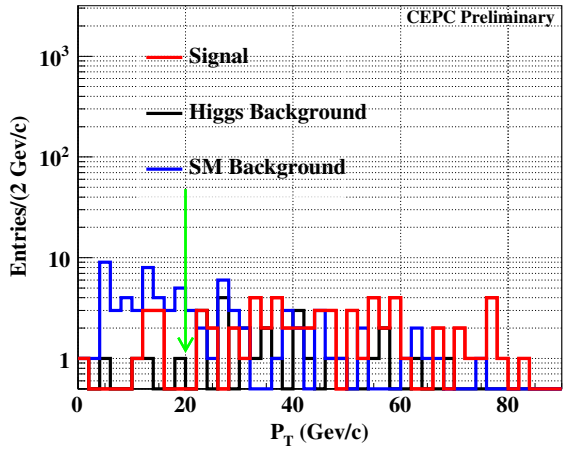

Figure 16: The distribution of transverse momentum

The event selection is showed in Table 16.

Category	Signal	ZH background	SM background
Total	192	37094	1303843
Validation of Pre-selection	104	21983	151498
$N_{ZPole} = 2; N_{Isolep} = 2; l_1 = e, l_2 = \mu$	80	111	245
$N_{Remain} < 5$	80	88	208
$10\ \mathrm{GeV}/c^2 < M^{e\mu}_{Inv} < 65\ \mathrm{GeV}/c^2$	76	73	169
$20\ \mathrm{GeV}/c^2 < M_{Missing} < 70\ \mathrm{GeV}/c^2$	65	28	70
$P_T > 20\ \mathrm{GeV}/c$	57	23	34
$\sqrt{(\frac{D0}{sigD0})^2 + (\frac{Z0}{sigZ0})^2} < 4$	53	3	3

Table 16: Cut chain of $eee\mu$ final state

Since the number of background after event selection is lower than 10, the detail of contained background would not be listed. According to Table 16, the events of signal are $N_{sig} = 53 \pm 8$ by counting, and efficiency of signal selection is 27.6%. The precision of this subchannel is

$$Accu. = \frac{\sqrt{S+B}}{S} = 15.1\%.$$

A.3 Analysis of $e^+e^- \to ZH, Z \to e^+e^-, H \to WW^* \to \mu\nu\mu\nu$ decay

In this channel, the main background is also eeZ process, and Z boson decay to a pair of μ. For the same reason mentioned before, transverse momentum of four leptons is applied.

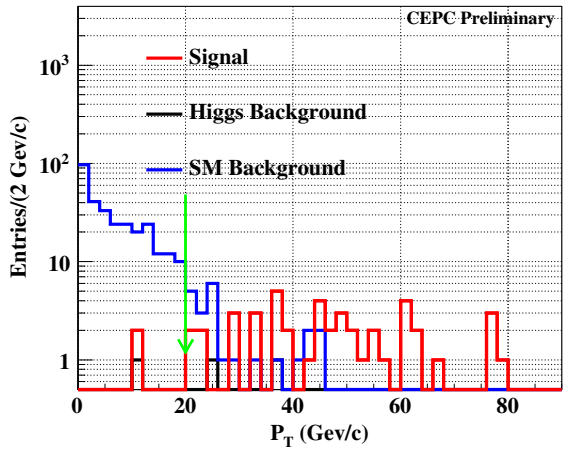

Figure 17: The distribution of transverse momentum

Events of eeZ process would be reduced a lot after p_T selection, as shown in Figure 17. The cut chain is showed in Table 17.

Category	Signal	ZH background	SM background
Total	102	37094	1303843
Validation of Pre-selection	58	21983	151498
$N_{ZPole} = 2; N_{Isolep} = 2; l_1 = \mu, l_2 = \mu$	57	92	4385
$N_{Remain} < 4$	57	50	4098
$5\ \mathrm{GeV}/c^2 < M^{\mu\mu}_{Inv} < 60\ \mathrm{GeV}/c^2$	53	41	1601
$20\ \mathrm{GeV}/c^2 < M_{Missing} < 65\ \mathrm{GeV}/c^2$	46	3	320
$P_T > 20\ \mathrm{GeV}/c$	44	2	23
$\sqrt{(\frac{D0}{sigD0})^2 + (\frac{Z0}{sigZ0})^2} < 4$	44	1	17

Table 17: Cut chain of $ee\mu\mu$ final state

After event selection, the main background and its number are shown in Table 18.

Decay Chain	Final States	Number of Events
$e^+e^- \to eeZ \to ee\mu\mu$	$2e, 2\mu$	17

Table 18: The main background and its number after event selection

Through counting, the events of signal is $N_{sig} = 44 \pm 8$, and the efficiency of signal selection is 43.1%. The precision of this channel is:

$$Accu. = \frac{\sqrt{S+B}}{S} = 18.2\%.$$

A.4 Analysis of $e^+e^- \to ZH, Z \to \mu^+\mu^-, H \to WW^* \to e\nu e\nu$ decay

Since the final states in this channel are the same as $e^+e^- \to ZH, Z \to e^+e^-, H \to WW^* \to \mu\nu\mu\nu$ decay channel, it's no doubt that their main background are the same, eeZ process. And transverse momentum of four leptons are also powerful to ruduce this background, as shown in Figure 18.

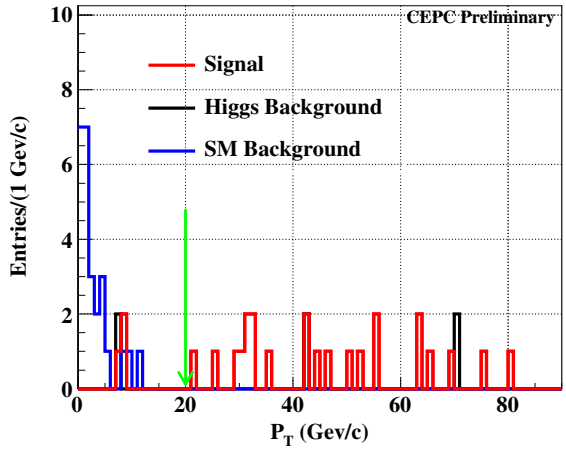

Figure 18: The distribution of transverse momentum

The detail of cut chain is shown in Table 19.

Category	Signal	ZH background	SM background
Total	89	35333	700311
Validation of Pre-selection	73	29479	117395
$N_{ZPole} = 2; N_{Isolep} = 2; l_1 = e, l_2 = e$	48	117	5964
$N_{Remain} < 4$	48	73	4968
$5\ \mathrm{GeV}/c^2 < M^{ee}_{Inv} < 45\ \mathrm{GeV}/c^2$	39	48	204
$20\ \mathrm{GeV}/c^2 < M_{Missing} < 65\ \mathrm{GeV}/c^2$	30	5	48
$\sqrt{(\frac{D0}{sigD0})^2 + (\frac{Z0}{sigZ0})^2} < 4$	26	2	26
$P_T > 20\ \mathrm{GeV}/c$	23	2	0

Table 19: Cut chain of $\mu\mu ee$ final state

Because the number of background is less than 10, the its detail would not be listed. According to Table 19 and through counting, the number of signal events is $N_{sig} = 23 \pm 5$. Efficiency of signal selection is 25.8%. The precision of this channel is:

$$Accu. = \frac{\sqrt{S+B}}{S} = 21.7\%$$

A.5 Analysis of $e^+e^- \to ZH, Z \to \mu^+\mu^-, H \to WW^* \to \mu\nu\mu\nu$ decay

There are four muons as the visible final state in this channel, therefore the ZZ process is the main background. Definitely, transverse momentum of four leptons is also useful to reduce this background, as shown in Figure 19.

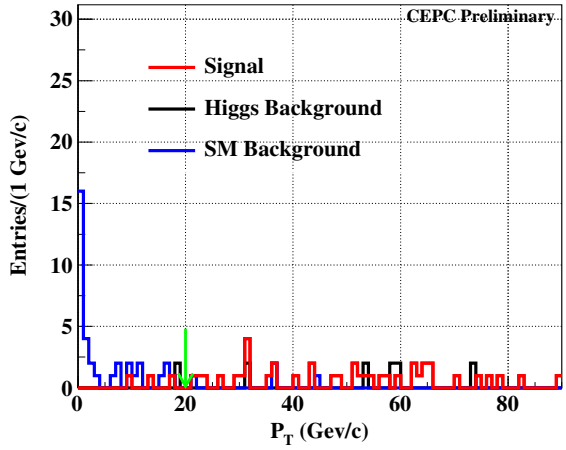

Figure 19: The distribution of transverse momentum

After the event selection, the cut chain is shown in Table 20.

Category	Signal	ZH background	SM background
Total	87	35333	700311
Validation of Pre-selection	68	29479	117395
$N_{ZPole} = 2; N_{Isolep} = 2; l_1 = \mu, l_2 = \mu$	66	133	2661
$N_{Remain} < 4$	63	71	2282
$5\ \mathrm{GeV}/c^2 < M_{Inv}^{\mu\mu} < 45\ \mathrm{GeV}/c^2$	53	55	375
$20\ \mathrm{GeV}/c^2 < M_{Missing} < 65\ \mathrm{GeV}/c^2$	43	12	63
$\sqrt{(\frac{D0}{sigD0})^2 + (\frac{Z0}{sigZ0})^2} < 4$	42	6	39
$P_T > 20\ \mathrm{GeV}/c$	39	5	4

Table 20: Cut chain of $\mu\mu\mu\mu$ final state

Because the number of background is less than 10, the its detail would not be listed. According to Table 20 and through counting, the number of signal events is $N_{sig} = 39 \pm 7$. Efficiency of signal selection is 44.8%. The precision of this channel is:

$$Accu. = \frac{\sqrt{S+B}}{S} = 17.9\%$$

B Analysis of the other semi-leptonic decay

In semi-leptonic decay channel, $eeH \to evqq$, $\mu\mu H \to evqq$ and $\mu\mu H \to \mu\nu qq$, these three channels are highly similar with $eeH \to \mu\nu qq$ channel, and the same variables have been applied in these three channel. Therefore, only the cut chain would be listed below, as well as the main background and its number of events. For $\nu\nu H \to \nu\nu evqq$ and $\nu\nu H \to \nu\nu\mu\nu qq$, they would be much different with the others due to the initial Z boson decay to two neotrinoes and there are only three visible pfos in the final states, so one of them would be introduced completely.

B.1 Analysis of $e^+e^- \to ZH, Z \to e^+e^-, H \to WW^*, WW^* \to evq\bar{q}$ decay

Table 21 shows the details of event selection, and Table 22 lists the main background in this channel.

Category	Signal	ZH background	SM background
Total	1177	35142	1303847
$N_{ZPole} = 2; N_{Isolep} = 1; N_{Jets} = 2; l = e$	882	1235	64595
Validation of Pre-selection	598	693	8437
$7 < N_{Remain} < 30$	567	208	961
$10\ \mathrm{GeV}/c^2 < M_{Inv}^{di-Jet} < 95\ \mathrm{GeV}/c^2$	542	136	662
$Btag < 0.9$	535	102	428
$M_{Missing} < 45\ \mathrm{GeV}/c^2$	523	50	393
$\sqrt{(\frac{D0}{sigD0})^2 + (\frac{Z0}{sigZ0})^2} < 9$	490	23	278
$p_T > 10\ \mathrm{GeV}/c$	435	13	61

Table 21: Cut chain of semi leptonic decay of $ZH \to ZWW^* \to eeevqq$

Decay Chain	Final States	Number of Events
$e^+e^- \to eeZ \to ee\tau\tau$	$2e, 2\tau$	11
$e^+e^- \to eeZ \to eeqq$	$2e, 2q$	46

Table 22: The main background and its number after event selection

There are some τ events in the background, and it could be reduced by a reliable $\tau-$finding. Although the number of ZH background events is larger than 10, it includes more than two parts, such as $ZH \to \nu\nu\tau\nu qq$ and $ZH \to b\bar{b}$. Therefore, the detail of ZH background would not be listed. According to this result, the number of signal events is $N_{sig} = 435 \pm 23$. Efficiency of signal selection is 37.0%. The precision is:

$$Accu. = \frac{\sqrt{S+B}}{S} = 5.3\%.$$

B.2 Analysis of $e^+e^- \to ZH, Z \to \mu^+\mu^-, H \to WW^*, WW^* \to evq\bar{q}$ decay

Table 23 shows the details of event selection, and Table 24 lists the main background in this channel.

Category	Signal	ZH background	SM background
Total	1108	33207	1303847
$N_{ZPole} = 2; N_{Isolep} = 1; N_{Jets} = 2; l = e$	842	961	23524
Validation of Pre-selection	739	789	3167
$7 < N_{Remain} < 30$	704	220	213
$10\ \mathrm{GeV}/c^2 < M_{Inv}^{di-Jet} < 95\ \mathrm{GeV}/c^2$	688	160	137
$Btag < 0.9$	683	120	83
$M_{Missing} < 45\ \mathrm{GeV}/c^2$	675	73	74
$\sqrt{(\frac{D0}{sigD0})^2 + (\frac{Z0}{sigZ0})^2} < 4$	580	25	21
$p_T > 4\ \mathrm{GeV}/c$	573	22	8

Table 23: Cut chain of semi leptonic decay of $ZH \to ZWW^* \to \mu\mu evqq$

Decay Chain	Final States	Number of Events
$e^+e^- \to ZH \to ZWW^* \to \mu\mu\tau\nu qq$	$2\mu, \tau, \nu, 2q$	21

Table 24: The main background and its number after event selection

In this channel, the main background is $ZH \to \mu\mu\tau\nu qq$ decay channel, and τ decay to a electron. As we all known, energy of electron which come from τ is much more lower than its from signal. Because of the few number of background, it's not useful to distinguish them. According to this result, the number of signal events is $N_{sig} = 573 \pm 25$. Efficiency of signal selection is 51.7%. The precision is:

$$Accu. = \frac{\sqrt{S+B}}{S} = 4.4\%.$$

B.3 Analysis of $e^+e^- \to ZH, Z \to \mu^+\mu^-, H \to WW^*, WW^* \to \mu\nu q\bar{q}$ decay

Table 25 shows the details of event selection, and Table 26 lists the main background in this channel.

Category	Signal	ZH background	SM background
Total	1105	33207	1303847
$N_{ZPole} = 2; N_{Isolep} = 1; N_{Jets} = 2; l = \mu$	970	1756	11007
Validation of Pre-selection	849	1494	1893
$7 < N_{Remain} < 30$	807	664	723
$10\ \mathrm{GeV}/c^2 < M_{Inv}^{di-Jet} < 95\ \mathrm{GeV}/c^2$	794	353	588
$Btag < 0.9$	787	149	238
$M_{Missing} < 45\ \mathrm{GeV}/c^2$	778	89	226
$\sqrt{(\frac{D0}{sigD0})^2 + (\frac{Z0}{sigZ0})^2} < 4$	772	32	184
$p_T > 4\ \mathrm{GeV}/c$	756	30	123

Table 25: Cut chain of semi leptonic decay of $ZH \to ZWW^* \to \mu\mu\nu qq$

Decay Chain	Final States	Number of Events
$e^+e^- \to ZH \to ZWW^* \to \mu\mu\tau\nu qq$	$2\mu, \tau, \nu, 2q$	22
$e^+e^- \to ZZ \to \mu\mu qq$	$2\mu, 2q$	117

Table 26: The main background and its number after event selection

There are some τ events in the ZH background, and it could be reduced by a reliable $\tau-$finding. According to this result, the number of signal events is $N_{sig} = 756 \pm 30$. Efficiency of signal selection is 68.4%. The precision is:

$$Accu. = \frac{\sqrt{S+B}}{S} = 4.0\%.$$

B.4 Analysis of $e^+e^- \to ZH, Z \to \nu\nu, H \to WW^*, WW^* \to \mu\nu q\bar{q}$ decay

Compared to the $\nu\nu qqqq$ channel, there are only three pfos in the final state. Therefore the conditions of pre-selection would be a little different after the number of pfos applied, shown in Table B.4 and Figure 20.

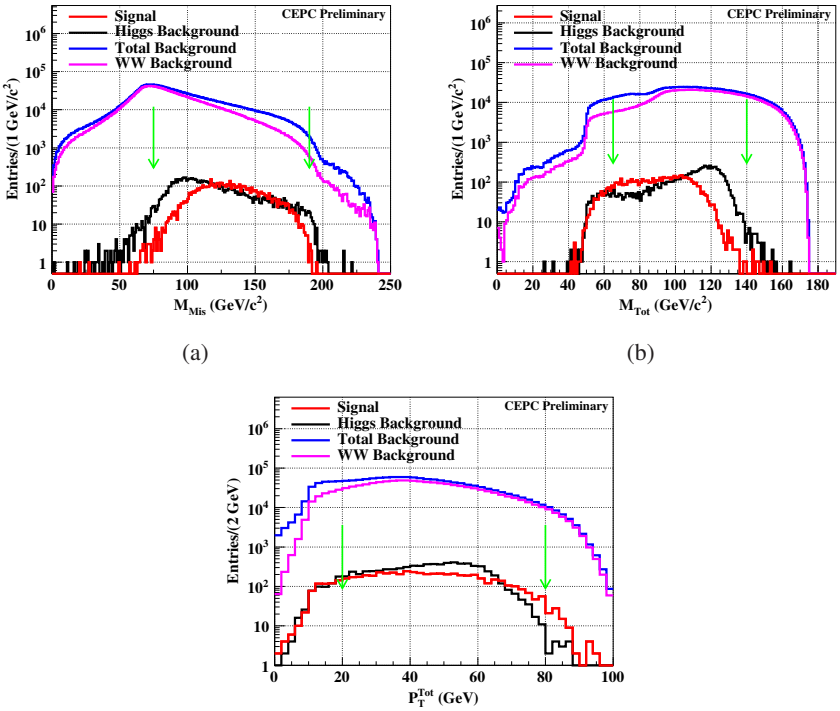

(a) (b)

(c)

Figure 20: The distribution of missing mass, total mass and total transverse momentum in full simulation in $\nu\nu\mu\nu qq$ channel. Compared to the $\nu\nu qqqq$ channel, upper missing mass should be lower, and visible mass should be shifted left. Transverse momentum would be same. Top: The left is missing mass of event. The right is total mass of event. Bottom: It is the distribution of total transverse momentum of event.

Process of signal	$\nu\nu H \to \nu\nu\mu\nu qq$
conditions of pre-selection	$65\ \mathrm{GeV}/c^2 < M_{Mis} < 225\ \mathrm{GeV}/c^2$ $M_{Tot} > 50\ \mathrm{GeV}/c^2$ $10\ \mathrm{GeV}/c < p_T < 100\ \mathrm{GeV}/c$
conditions of validation	$75\ \mathrm{GeV}/c^2 < M_{Mis} < 140\ \mathrm{GeV}/c^2$ $65\ \mathrm{GeV}/c^2 < M_{Tot} < 140\ \mathrm{GeV}/c^2$ $20\ \mathrm{GeV}/c < p_T < 80\ \mathrm{GeV}/c$

Table 27: Conditions of pre-selection in MC and validation in full simulation of $\nu\nu H \to \nu\nu\mu\nu qq$ process

Since it is a semi-leptonic decay channel, the number of particles except for the isolated lepton, shown in Figure 21(a) would be larger than pure leptonic decay channel and lower than pure hadronic decay channel.

To reduce the events of τ and b background, the vertex parameter is a useful condition by requiment of $\sqrt{(\frac{D_0}{sigD_0})^2 + (\frac{Z_0}{sigZ_0})^2}$, shown in Figure 21(b).

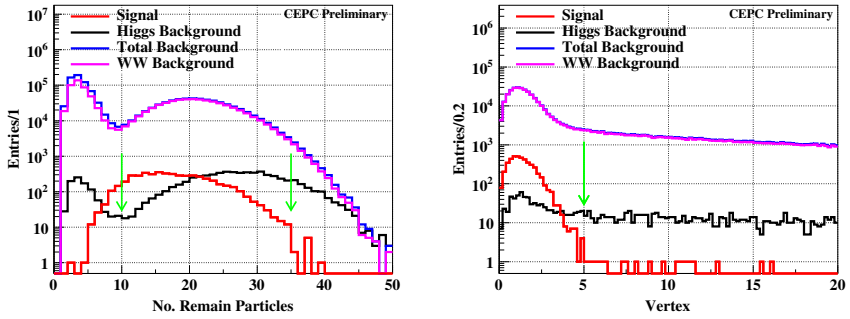

(a) (b)

Figure 21: The distribution of particles number and the distance of μ and IP in $\nu\nu\mu\nu qq$ channel.

The main background is WW channel right now. In order to reduce this background, a 2-dimensional distribution would be applied. As shown in Figure 22, the events in two regions, two black boxes in the plot, would be survived.

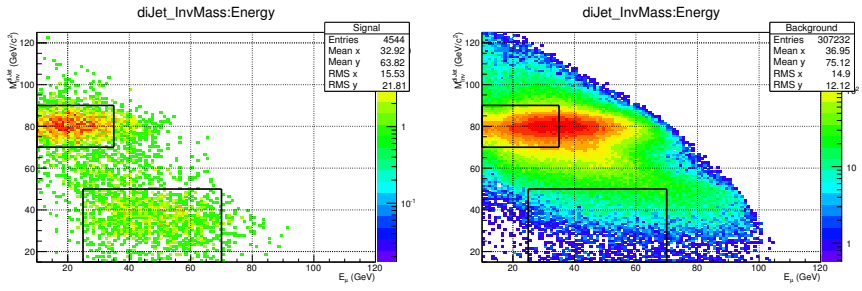

(a) (b)

Figure 22: The distribution of lepton energy vs. di-jet invariant mass in $\nu\nu\mu\nu qq$ channel. The left plot is the signal process and the right one is the background process which includes ZH background and SM background. X-axis is the energy of lepton and Y-axis is the invariant mass of di-jet.

Due to the main background is WW background, the recoil mass of di-jet is another powerful condition to reduce, as shown in Figure 23. The recoil mass of some background events would be near to the W mass.

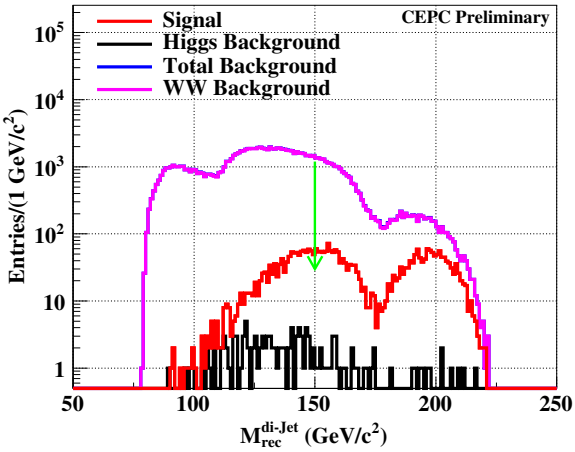

Figure 23: The distribution of recoil mass of di-jet.

Then, some variables would be put into TMVA for test and training, and the BDT(Boosted decision trees) method is applied. The Figure 24 shows the correlation matrix of signal and events, and the result of test and training samples is shown in Figure 25. The input variables would be introduced below:

- WWAngle: This is the angle of WW boson, one of the W bosons is conbined by di-jet, and the other one is lepton.
- RecE: The energy of the isolated lepton.
- Area: Three vectors of 3-dimensional momentum, A, B and C, could be given by three pfos in the event. Vab is equal to A minus B. Vbc is equal to B minus C. Vca is equal to C minus A. And a triangle would be constructed by these three vectors, Vab, Vbc and Vca. The area is the area of this triangle.
- NorCosThe: It is the polar angle of area which is mentioned before.
- Z0 and D0: They are the vertex parameter of lepton.
- diJet_angle: This is the angle between di-jet.
- CtagOne: This is the probobility of c quark tagging for the more energetic jet.
- TotalPt and VisMass: These two variables are introduced in the pre-selection.

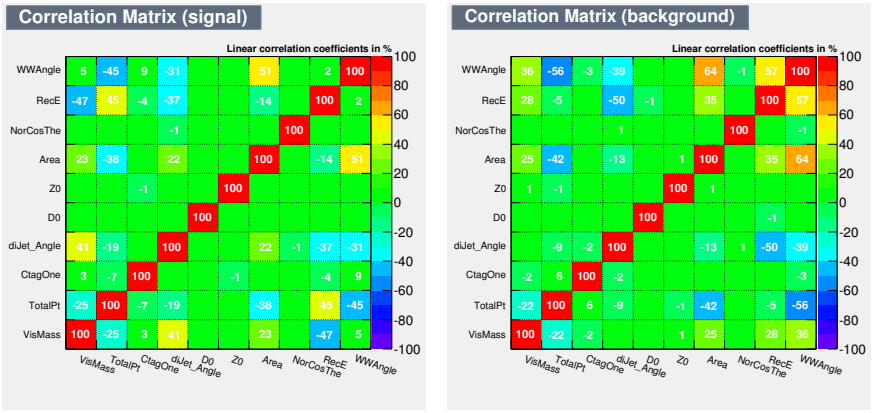

(a) (b)

Figure 24: The correlation matrix in $\nu\nu\mu\nu qq$ channel. The left plot is the signal process and the right one is the background process which includes ZH background and SM background.

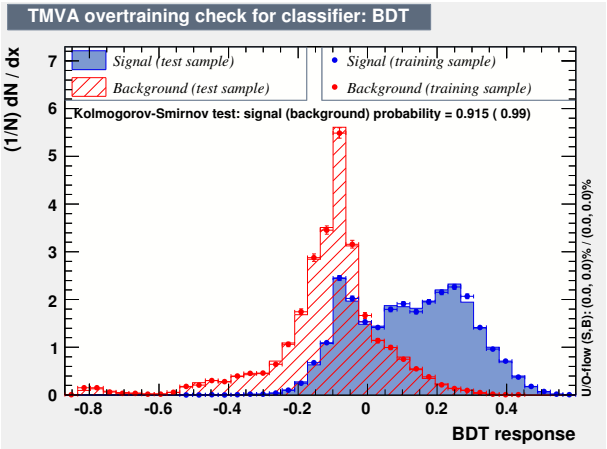

Figure 25: The result of BDT for test and training samples.

After event selection, the detail of each step is shwon in Table 28 and the main background is listed in Table 29.

Category	Signal	ZH background	SM background
Total	7057	217161	23469024
$N_{ZPole} = 2; N_{Isolep} = 1; N_{Jets} = 2; l = \mu$	6532	9006	3087607
Validation of Pre-selection	5099	7291	1232771
$10 < N_{Remain} < 35$	4564	5430	581219
$\sqrt{(\frac{D0}{sigD0})^2 + (\frac{Z0}{sigZ0})^2} < 5$	4538	689	306543
$E_\mu Vs.M_{Inv}^{di-jet}$	3322	131	113762
$M_{Rec}^{di-jet} > 150\ \mathrm{GeV}/c^2$	2200	39	24669
$BDT > 0.2$	790	4	315

Table 28: Cut chain of semi leptonic decay of $ZH \to ZWW^* \to \nu\nu\mu\nu qq$

Decay Chain	Final States	Number of Events
$e^+e^- \to WW \to \tau\nu qq$	$\tau, 2q$	32
$e^+e^- \to WW \to \mu\nu qq$	$\mu, 2q$	274

Table 29: The main background and its number after event selection

Through counting, the number of signal is $N_{sig} = 790 \pm 33$, and the efficiency of signal selection is 11.2%. According to this result, the precision of this channel is:

$$Accu. = \frac{\sqrt{S+B}}{S} = 4.2\%.$$

B.5 Analysis of $e^+e^- \to ZH, Z \to \nu\nu, H \to WW^*, WW^* \to e\nu q\bar{q}$ decay

The process of this analysis is much similar with $\nu\nu\mu\nu qq$ channel, and the applied variables are also same. The same technique, BDT of TMVA, is also applied but the variables are little different with $\nu\nu\mu\nu qq$. The Figure 26 shows the correlation matrix of signal and events, and the result of test and training samples is shown in Figure 27. The variables for BDT would be introduced below:

- WWAngle: This is the angle of WW boson, one of the W bosons is conbined by di-jet, and the other one is lepton.
- diJet_recoil: The recoil mass of di-jet.
- Area: Three vectors of 3-dimensional momentum, A, B and C, could be given by three pfos in the event. Vab is equal to A minus B. Vbc is equal to B minus C. Vca is equal to C minus A. And a triangle would be constructed by these three vectors, Vab, Vbc and Vca. The area is the area of this triangle.
- NorCosThe: It is the polar angle of area which is mentioned before.
- Z0: It is the vertex parameter of lepton.
- diJet_angle: This is the angle between di-jet.
- CtagOne and CtagTwo: They are the probobilitis of c quark tagging for two jet.
- TotalPt and VisMass: These two variables are introduced in the pre-selection.

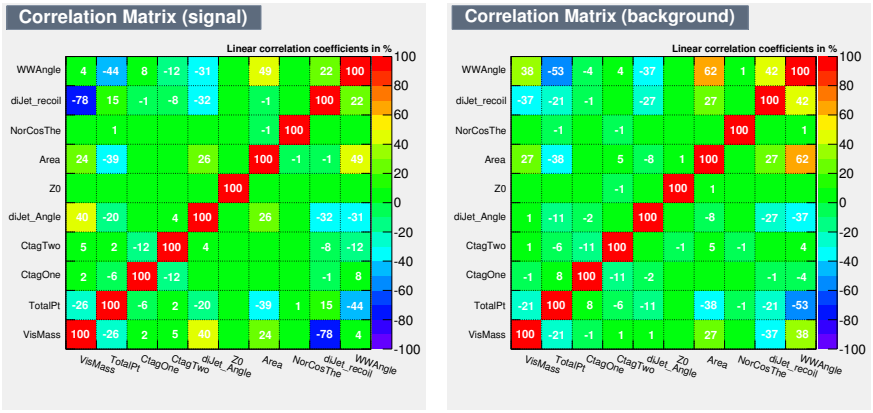

(a) (b)

Figure 26: The correlation matrix in *vvevqq* channel. The left plot is the signal process and the right one is the background process which includes ZH background and SM background.

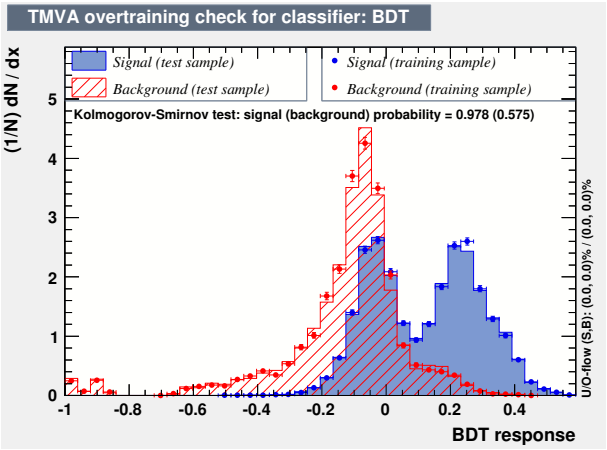

Figure 27: The result of BDT for test and training samples.

The detail of each step for event selection is shown in Table 30.

Category	Signal	ZH background	SM background
Total	6966	217252	23469024
$N_{ZPole} = 2; N_{Isolep} = 1; N_{Jets} = 2; l = \mu$	5730	3495	3019180
Validation of Pre-selection	4468	2388	1258539
$10 < N_{Remain} < 35$	3971	1312	528845
$\sqrt{(\frac{D0}{sigD0})^2 + (\frac{Z0}{sigZ0})^2} < 5$	3511	316	261404
$E_\mu Vs.M_{Inv}^{di-jet}$	2587	63	93618
$M_{Rec}^{di-jet} > 150\ \mathrm{GeV}/c^2$	1764	31	20591
$BDT > 0.2$	680	4	359

Table 30: Cut chain of semi leptonic decay of $ZH \to ZWW^* \to vvevqq$

The below plot,Table 31, is listed the main background which number of events are larger than 10.

Decay Chain	Final States	Number of Events
$e^+e^- \to WW \to \tau\nu qq$	$\tau, 2q$	13
$e^+e^- \to e\nu W \to e\nu qq$	$e, 2q$	344

Table 31: The main background and its number after event selection

Through counting, the number of signal is $N_{sig} = 680 \pm 32$, and the efficiency of signal selection is 9.8%. According to this result, the precision of this channel is:

$$Accu. = \frac{\sqrt{S+B}}{S} = 4.7\%.$$

C Isolated leptons' condition

Isolated leptons tagging is a key in WW^* analysis, especially in jets environment, so a good iaolated leptons algorithm could decide our analysis accuracy. We will introduce the isolated leptons algorithm below:

There are two key conditions. The first one is lepton identification that a good PFA could help us. The second is isolated conditions, cone angle of lepton and the ratio of energy in cone angle and lepton's energy, shown in Table 32.

E_{lepton}	Leptons' flavor	Full-leptonic Decay		Semi-leptonic Decay	
		Cone Angle[rad]	E_{Cone}/E_{Lepton}	Cone Angle[rad]	E_{Cone}/E_{Lepton}
5 GeV – 10 GeV	Muon	0.15	0.25	0.15	0.7
	Electron	0.3	1.1	0.3	0.9
10 GeV – 15 GeV	Muon	0.15	0.35	0.15	0.25
	Electron	0.3	0.75	0.3	0.75
> 15 GeV	Muon	0.15	0.3	0.15	0.25
	Electron	0.25	0.55	0.25	0.6

Table 32: Isolated lepton condition